Iraqi Journal of Physics, 2018 *Vol.16, No.39, PP. 103-116*

DOI: 10.20723/ijp.16.39.103-116

Study of nuclear structure for carbon isotopes using local scale transformation technique in shell model

Saja H. Mohammed and Arkan R. Ridha

Department of Physics, College of Science, University of Baghdad, Baghdad, Iraq

E-mail: Saja.alazawi94@gmail.com

Abstract

This work is devoted to study the properties of the ground states such as the root-mean square (rms) proton, charge, neutron and matter radii, nuclear density distributions and elastic electron scattering charge form factors for Carbon Isotopes (^{9}C, ^{12}C, ^{13}C, ^{15}C, ^{16}C, ^{17}C, ^{19}C and ^{22}C). The calculations are based on two approaches; the first is by applying the transformed harmonic-oscillator (THO) wavefunctions in local scale transformation (LST) to all nuclear subshells for only ^{9}C, ^{12}C, ^{13}C and ^{22}C. In the second approach, the ^{9}C, ^{15}C, ^{16}C, ^{17}C and ^{19}C isotopes are studied by dividing the whole nuclear system into two parts; the first is the compact core part and the second is the halo part. The core and halo parts are studied using the radial wave functions of HO and THO radial wavefunctions, respectively. For ^{9}C, ^{12}C and ^{13}C isotopes, the no-core shell model (NCSM) are studied using the Warburton-Brown interaction. Very good agreements are obtained for the calculated density distributions and form factors in comparison with experimental data.

Key words

Exotic nuclei, nuclear density distributions, elastic electron scattering form factors, proton, charge.

Article info.

Received: Jul. 2018
Accepted: Sep. 2018
Published: Dec. 2018

دراسة التركيب النووي لنظائر الكربون باستخدام تقنية تحويل المقياس الموضعي في نموذج القشرة

سجى حازم محمد و أركان رفعه رضا

قسم الفيزياء، كلية العلوم، جامعة بغداد، بغداد، العراق

الخلاصة

هذا العمل خصص لدراسة خصائص المستويات الأرضية مثل انصاف الاقطار البروتونية والشحنية والنيوترونية والنيوكليونية وتوزيعات الكثافة النووية وعوامل التشكل الشحنية للاستطارة الالكترونية المرنة لنظائر الكاربون المستقرة وغير المستقرة (^{9}C,^{12}C,^{13}C, ^{15}C, ^{16}C, ^{17}C, ^{19}C, ^{22}C). استندت الحسابات على طريقتين؛ الاولى تمت بواسطة استخدام الدوال الموجية المحولة لجهد المتذبذب التوافقي باستخدام تقنية تحويل المقياس الموضعي على جميع الاغلفة النووية وفقط للنظائر (^{9}C,^{12}C,^{13}C, ^{22}C). في الطريقة الثانية، بعض نظائر الكاربون (^{9}C,^{15}C,^{16}C, ^{19}C) درست بتقسيمها الى جزئين; الاول هو جزء القلب والثاني هو جزء الهالة. جزء القلب وجزء الهالة درس باستخدام الدوال الموجية القطرية لجهد المتذبذب التوافقي البسيط (HO) والدوال الموجية للمتذبذب التوافقي المحولة (THO) بالتتابع. لنظائر الكاربون (^{9}C,^{12}C, ^{13}C) تم تطبيق الدوال الموجية على جميع القشر الثانوية بنموذج القشرة عديم القلب باستخدام تفاعل واربيرتين-براون. وجد بان توزيعات الكثافة وعوامل التشكل المحسوبة هي بتطابق جيد جدا مقارنة مع القيم العملية.

Introduction

The study of density distributions are very important in studying the nuclear structure and nuclear reactions [1]. One of the most fundamental properties of atomic nuclei are the nuclear neutron, proton, charge and matter root-mean square (rms) radii.

Over the years, an information about charge densities can be obtained by different approaches, started from elastic electron scattering and muonic atoms (μ−) [2]. The density distributions and matter radii are deduced from interaction or reaction cross sections [3]. The proton and neutron rms radii are essential for extracting the neutron skin thickness [4]. The charge radii of unstable isotopes are a variable from isotope shift measurement [5]. The discovery of halo structure was one of the most striking indications of the changes in structure for exotic nuclei. The extraordinary interaction cross section and rms matter radius was an outstanding property founded by Tanihata et al., in 1985 for some exotic nuclei [3]. The nuclear halo is a structure with a dilute matter distribution and characteristic such as: a very loosely bound valence nucleon and short lifetimes. The nucleons in halo nuclei held in a shallow potential well can tunnel into the surrounding space with significant probability to be found at distances much greater than the nuclear radius and can have wavefunctions that extend to distances much larger than the range of the interaction [6]. The nuclear halo is related to low separation energy of the last proton(s) or neutron(s) in comparison with the rest of other nucleons [7]. In addition, the centrifugal barrier is preferred to be low, i.e., the orbital quantum numbers are either $l = 0$ or $l = 1$ [8]. Over the last few decades, experiments at radioactive ion beam facilities have revealed that several drip-line nuclei have a halo structure divided into a "core" of normal nuclear density and one or more protons or neutrons whose probability distribution extends far beyond the range of nuclear interactions [9]. The first idea of halo, which was suggested by Jonson and Hansen [7] was appeared when the binding energy is sufficiently small. It appears in loosely bound. Two-neutron halo nuclei, such as ^{6}He and ^{11}Li have the remarkable property that none of their two-body subsystems are bound. Thus, ^{6}He can be modeled as a bound three-body $\alpha + n + n$ system despite there being no bound states of *n*+*n* (the dineutron). Such nuclei have been dubbed 'Borromean', since the observation of the ^{11}Li halo, special attention has been paid to nuclei showing a halo state consisting of two neutrons. In ref. [10], the compilation of experimental matter radii of nuclei in *sp* and *sd* shells are presented. These two-neutron halo nuclei are three-body systems with no bound binary sub-system and are referred to as Borromean nuclei [11]. In ref. [12], the density distributions and rms radii are calculated using LST for some nuclei with limited agreements with experimental data. In their results, the filling numbers of pure state are adopted.

In this work, the radial wavefunctions of THO is used to reproduce the long tail characteristic of exotic nuclei. The bare HO wavefunction is not sufficient to reproduce such characteristic, therefore, the LST are used to get rid of such defect.

Theoretical basis

The radial multipole transition density operator of order J (multipolarity) and projection M can be written as [13]:

$$\hat{\rho}_{JM,t_z} = \sum_{i=1}^{x} \frac{\delta(r-r_i)}{r_i^2} Y_{JM}(\theta_i, \phi_i) \qquad (1)$$

where x denotes the number of neutrons (N, $t_z = -1/2$) or protons (Z, $t_z = 1/2$). The nuclear matrix element to Eq. (1) between initial and final nuclear states can be written as [13]:

$$\rho_{J,t_z}(r) = \frac{1}{\sqrt{4\pi}} \frac{1}{\sqrt{2J_i+1}} \sum_{ab} X_{b,a,t_z}^{J_f, J_i, J} \langle j_b \| Y_J \| j_a \rangle R_{n_b l_b}(r, b_{t_z}) R_{n_a l_a}(r, b_{t_z}) \quad (2)$$

where $R_{nl}(r, b_{t_z})$ represents the radial wavefunctions. The J_i and J_f are the total spin of the nucleus in the initial and final states. Besides, a and b denote the single-particle quantum numbers of initial and final states (nlj; n, l and j represent the principal, orbital and total spin quantum numbers of a single nucleon, respectively). $X_{b,a,t_z}^{J_f, J_i, J}$ is the weight of transition calculated from nuclear shell model by using *Nushell* code [14] for a given effective interaction and model space. For ground density distribution ($J_f = J_i, a = b \; and \; J = 0$), Eq. (2) can be written as:

$$\rho_{J=0,t_z}(r) = \frac{1}{4\pi} \sqrt{\frac{2j_a+1}{2J_i+1}} \sum_a X_{a,a,t_z}^{J_i, J_i, J=0} \left| R_{n_a l_a}(r, b_{t_z}) \right|^2 \quad (3)$$

The nuclear density distributions of point neutron and proton for halo nuclei are calculated in two methods; the first is by using Eq. (3), the second is by writing the density distribution as a sum of two main parts; the core ($\rho_{J=0,t_z}^{core}(r)$) and the halo ($\rho_{J=0,t_z}^{halo}(r)$) as follows [15]:

$$\rho_{J=0,t_z}(r) = \rho_{J=0,t_z}^{core}(r) + \rho_{J=0,t_z}^{halo}(r) \quad (4)$$

In Eq. (4), the core and halo parts are calculated respectively by using the following two formula:

$$\rho_{J=0,t_z}^{core}(r) = \frac{1}{4\pi} \sum_{nl} \xi_{nl,t_z}^{core} \left| R_{nl}(r, b_{t_z}) \right|^2 \quad (5)$$

and

$$\rho_{J=0,t_z}^{halo}(r) = \frac{1}{4\pi} \sum_{nlj} \xi_{nl\,t_z}^{halo} \left| R_{nl}(r, b_{t_z}) \right|^2 \quad (6)$$

where ξ_{nl,t_z}^{core} and $\xi_{nl\,t_z}^{halo}$ represent the neutrons or protons occupation number in the nl shells of core and halo respectively. In the present work, ξ_{nl,t_z}^{core} takes integer numbers as predicted by simple shell model. $\rho_{J=0,t_z}^{halo}$ takes assumed fractional real numbers. Due to the Gaussian fall off behaviour of the radial wavefunction of HO potential. The $R_{nl}(r, b_{t_z})$ in Eq. (3) and (6) are calculated by using the transformed HO (THO) radial wavefunctions based on LST as follows [16]:

$$R_{nl}^{THO}(r, b_{t_z}) = \frac{f(r)}{r} \sqrt{\frac{df(r)}{dr}} R_{nl}(f(r), b_{t_z}) \quad (7)$$

and the function $f(r)$ is [16]:

$$f(r) = \left[\frac{1}{\left(\frac{1}{r}\right)^m + \left(\frac{1}{\gamma\sqrt{r}}\right)^m} \right]^{\frac{1}{m}} \quad (8)$$

The $f(r)$, in Eqs. (7) and (8), represent a function chosen so as to reproduce the proper asymptotic condition (exponential shape) for the density distribution at large r, besides that it leaves the interior shape of density unchanged [17]. m and γ in Eq. (10) are an integer and real numbers controls how sharply the tail of wave function will be. Therefore, Eqs. (3) and (4) become, respectively as follows:

$$\rho_{J=0,t_z}(r) = \frac{1}{4\pi} \sqrt{\frac{2j_a+1}{2J_i+1}} \sum_a X_{a,a,t_z}^{J_i, J_i, J=0} \left| R_{nl}^{THO}(r, b_{t_z}) \right|^2 \quad (9)$$

and

$$\rho_{J=0,t_z}(r) = \frac{1}{4\pi} \sum_{nl} \xi_{nl,t_z}^{core} \left| R_{nl}(r, b_{t_z}) \right|^2 + \frac{1}{4\pi} \sum_{nlj} \xi_{nl\,t_z}^{halo} \left| R_{nl}^{THO}(r, b_{t_z}) \right|^2 \quad (10)$$

The main two methods in Eq. (9) and (10) are denoted by LST and HO+LST, respectively. The matter density distributions can be written as:

$$\rho_m^{core}(r) = \rho_{J=0,t_z=1/2}^{core}(r) + \rho_{J=0,t_z=-1/2}^{core}(r) \quad (12)$$

and

$$\rho_{J=0,m}^{halo}(r) = \rho_{J=0,t_z=+/-1/2}^{halo}(r) \quad (13)$$

The total charge density distribution $\rho_{ch}(r)$ (CDD) is coming from protons and neutrons as follows:

$$\rho_{ch}(r) = \rho_{ch,t_z=1/2}(r) + \rho_{ch,t_z=-1/2}(r) \quad (14)$$

The first and second terms in Eq.(14) are obtained by taking the folding of single proton/neutron charge density (ρ_{pr}/ρ_{neu}) into the distribution of the point proton/neutron density in Eqs. (9) or (10) as follows:

$$\rho_{ch,t_z=1/2}(r) = \int \rho_{J=0,t_z=1/2}(r)\rho_{pr}(\boldsymbol{r} - \boldsymbol{r'})d\boldsymbol{r'} \quad (15)$$

and

$$\rho_{ch,t_z=-1/2}(r) = \int \rho_{J=0,t_z=-1/2}(r)\rho_{neu}(\boldsymbol{r} - \boldsymbol{r'})d\boldsymbol{r'} \quad (16)$$

$\rho_{pr}(\vec{r})$ [18] and $\rho_{neu}(\vec{r})$ [19] takes, respectively the following forms:

$$\rho_{pr}(r) = \frac{1}{(\sqrt{\pi}a_{pr})^3} e^{\left(\frac{-r^2}{a_{pr}^2}\right)} \quad (17)$$

and

$$\rho_{neu}(r) = \frac{1}{(\pi r_i^2)^{3/2}} \sum_1^2 \theta_i \, e^{-r^2/r_i^2} \quad (18)$$

In Eq. (17), $a_{pr} = 0.65\ fm$ [18] to reproduce the experimental charge rms radius of the proton ($\langle r^2\rangle_{pr}^{1/2} = \left(\frac{3}{2}\right)^{1/2} a_{pr} \approx 0.8\ fm$). In Eq. (18), the parameter θ_i and r_i are given in Table 1.

Table 1: Parameters of the neutron charge distributions.

θ_1	1
θ_2	-1
r_1^2 (fm^2)	0.469
r_2^2 (fm^2)	0.546

The rms radii of neutron, proton and matter are calculated from [20]:

$$\langle r^2\rangle_X^{1/2} = \sqrt{\frac{4\pi}{X}\int_0^\infty \rho_{J=0,X}(r)r^2 dr} \quad (19)$$

where X stands for N (number of neutrons), Z (atomic number), and A (mass number), respectively. The rms charge radii are calculated from:

$$\langle r^2\rangle_{ch}^{1/2} = \sqrt{\frac{4\pi}{Z}\int_0^\infty \rho_{J=0,ch}(r)r^2 dr} \quad (20)$$

Finally, the longitudinal electron scattering form factors in the first Born approximation can be written as [21, 22]:

$$F_{J,ch}^C(q) = \frac{1}{Z}\sqrt{\frac{4\pi}{(2J_i+1)}}\sum_{t_z}\langle J_f \| \boldsymbol{O}_J^C(q,t_z)\| J_i\rangle f_{t_z}(q) \quad (21)$$

or

$$F_{J,ch}^C(q) = \sum_{t_z} F_J^C(q,t_z) f_{t_z}(q) \quad (22)$$

where

$$F_J^C(q,t_z) = \frac{1}{Z}\sqrt{\frac{4\pi}{(2J_i+1)}}\langle J_f \| \boldsymbol{O}_J^C(q,t_z)\| J_i\rangle \quad (23)$$

since,

$$F_{J,ch}^C(q,t_z) = F_J^C(q,t_z) f_{t_z}(q) \quad (24)$$

Therefore, Eq. (24) can be written as:

$$F^{C}_{J,ch}(q) = \sum_{t_z} F^{C}_{J,ch}(q,t_z) \quad (25)$$

where q represents the momentum transfer from electron to nucleus. $|J_i\rangle$ and $|J_f\rangle$ are initial and final states of the nucleus. $f_{t_z}(q)$ is the charge form factor of a single proton and neutron given by taking Fourier transforms to Eqs. (17) and (18), respectively. $\boldsymbol{O}^{C}_{J,t_z=1/2}(q)$ represents the Coulomb multipole operator of the longitudinal electron scattering given by [21]:

$$\boldsymbol{O}^{C}_{JM_J}(q,t_z) = \int j_J(qr)\, Y_{JM_J}(\Omega_r)\hat{\rho}_{t_z}(\vec{r}) \quad (26)$$

$$\hat{\rho}_{t_z}(\vec{r}) = \sum_{i=1}^{x} e_{t_z}\, \delta(\vec{r} - \vec{r}_i) \quad (27)$$

The reduced matrix element in Eqs.(21) and (23) can be written in terms of the reduced matrix element of a single nucleon matrix element as:

$$\langle J_f \| \boldsymbol{O}^{C}_{J}(q,t_z) \| J_i \rangle = \sum_{ab} X^{J_i J_f J}_{a,b,p/n} \langle b, t_z \| O^{C}_{J}(q,r,t_z) \| a, t_z \rangle \quad (28)$$

where

$$O^{C}_{J}(q,r,t_z) = e_{t_z} j_J(qr) Y_J(\Omega_r) \quad (29)$$

The single nucleon matrix element in Eq. (28) is given by:

$$\langle b, t_z \| O^{C}_{J}(q,r,t_z) \| a, t_z \rangle = e_{t_z} \langle n_b l_b | j_J(qr) | n_a l_a \rangle \left\langle \left(\frac{l_b 1}{2}\right) j_b \| Y_J(\Omega_r) \| \left(\frac{l_a 1}{2}\right) j_a \right\rangle \quad (30)$$

Eq. (21) can be written as [21]

$$\left|F^{C}_{J,ch}(q)\right| = \frac{1}{Z}\sqrt{\frac{4\pi}{(2J_i+1)}} \left| \int_0^{\infty} j_J(qr)\, \rho_{J,ch}(r) r^2 dr \right| \quad (31)$$

where $j_J(qr)$ and $\rho_{ch,J}(r)$ are spherical Bessel function and charge transition density distribution, respectively.

For $J = 0$, Eq. (31) can be written as

$$\left|F^{C}_{ch}(q)\right| = \frac{1}{Z}\sqrt{\frac{4\pi}{(2J_i+1)}} \left| \int_0^{\infty} j_0(qr)\, \rho_{ch}(r) r^2 dr \right| \quad (32)$$

Results and discussion

One of the important techniques to study the unstable nuclei and the long tail characteristic associated to the halo nuclei is the LST.

The calculations are established on two major techniques; the first is denoted by LST where the THO is applied to all subshells of the nuclei ^{9}C, ^{12}C, ^{13}C and ^{22}C. The second one is called HO+LST applied to the nuclei ^{9}C, ^{15}C, ^{16}C, ^{17}C and ^{19}C, where the radial wavefunctions of HO potential and THO are applied to the core and halo parts of the aforementioned nuclei, respectively. Besides, the results of the above two techniques are compared with the results of the HO calculations to show the defect of such bare radial wavefunctions in studying the halo nuclei. The properties of carbon isotopes ^{9}C, ^{12}C, ^{13}C, ^{15}C, ^{16}C, ^{17}C, ^{19}C and ^{22}C are shown in Table 2.

In Table 3, the size parameters (b_p and b_n), occupation numbers, m and $\gamma_{p,n}$ for Carbon isotopes (^{9}C, ^{15}C, ^{16}C, ^{17}C and ^{19}C) using HO+LST technique. In Table 4, the size parameters ($\boldsymbol{b_p}$ and $\boldsymbol{b_n}$), occupation numbers, m and $\gamma_{p,n}$ for Carbon isotopes ^{12}C, ^{13}C and ^{22}C using LST technique.

Table 2: Properties of carbon isotopes ^{9}C , ^{12}C, ^{13}C, ^{15}C, ^{16}C, ^{17}C, ^{19}C and ^{22}C.

$^{A}_{Z}X_{N}$	J^{π} [23]	Half-Life Time [23]	Type [24]	Separation Energies in MeV[25]
$^{9}_{6}C_{3}$	3/2^{-}	126.5 ms	1p-halo	$S_p = 1.299$
$^{12}_{6}C_{6}$	0^{+}	Stable	Stable	S_p =15.956 $S_n = 18.720$
$^{13}_{6}C_{7}$	1/2^{-}	Stable	Stable	$S_p = 17.533$ $S_n = 4.946$
$^{15}_{6}C_{9}$	1/2^{+}	2.4495 s	1n-halo	$S_n = 1.218$
$^{16}_{6}C_{10}$	0^{+}	0.747 s	2n-halo	S_{2n} =5.468
$^{17}_{6}C_{11}$	3/2^{+}	193 ms	1n-halo	$S_n = 0.734$
$^{19}_{6}C_{13}$	1/2^{+}	46.2 ms	1n-halo	$S_n = 0.580$
^{22}C	0^{+}	6.1 ms	2n-halo	S_{2n} =0.035

Table 3: The HO size parameters, occupation numbers and $\gamma_{p,n}$ for Carbon isotopes ^{9}C, ^{15}C, ^{16}C, ^{17}C and ^{19}C using HO+LST technics.

$^{A}_{Z}X_{N}$	$b_p(fm)$	$b_n(fm)$	nl_j	Occupation number	m	γ_p (fm^{-1})	γ_n (fm^{-1})
$^{9}_{6}C_{3}$	1.639	1.599	$1P_{1/2}$	1.0	16	1.442	1.208
$^{15}_{6}C_{9}$	1.59	1.6	$1d_{5/2}$	0.35	26	2.19	1.543
			$1d_{3/2}$	0.05			
			$2S_{1/2}$	0.6			
$^{16}_{6}C_{10}$	1.604	1.61	$1d_{5/2}$	0.7	26	1.376	1.503
			$1d_{3/2}$	0.2			
			$2S_{1/2}$	1.1			
$^{17}_{6}C_{11}$	1.645	1.799	$1d_{5/2}$	0.5	26	2.270	1.993
			$1d_{3/2}$	0.2			
			$2S_{1/2}$	0.3			
$^{19}_{6}C_{13}$	1.631	1.736	$1d_{5/2}$	0.2	26	2.255	1.277
			$1d_{3/2}$	0.1			
			$2S_{1/2}$	0.7			

Table 4: The HO size parameters and $\gamma_{p,n}$ for Carbon isotopes ^{12}C , ^{13}C and ^{22}C.

$^{A}_{Z}X_{N}$	$b_p(fm)$		$b_n(fm)$		nl_j		m	γ_p (fm^{-1})	γ_n (fm^{-1})
$^{12}_{6}C_6$	1.594	LST	1.594	LST	*Spsdpf*		24	2.599	2.599
	1.456	Assumed filling no.	1.456	Assumed filling no.	spsdpf	Assumed no.			
					$1S_{1/2}$	1.0			
					1P3/2	3.7			
					1d5/2	0.8			
					2S1/2	0.1			
					1f7/2	0.2			
					2P3/2	0.2			
$^{13}_{6}C_7$	1.563	LST	1.652	LST	*Spsdpf*		8	2.375	2.512
	1.419	Assumed filling no.	1.443	Assumed filling no.	spsdpf	Assumed no.			
					$1S_{1/2}$	1.0			
					1P3/2	3.7			
					1d5/2	0.8			
					2S1/2	0.1			
					1f7/2	0.3			
$^{22}_{6}C_{16}$	2.1	Assumed filling no.	2.8	Assumed filling no.	spsdpf	Assumed no.	14	2.908	3.879
					$1S_{1/2}$	2.0			
					1P3/2	4.0			
					1P1/2	2.0			
					1d5/2	1.8			
					2S1/2	2.0			
					2P3/2	2.6			
					2P1/2	1.6			

The calculated proton, charge, neutron, matter rms radii for Carbon isotopes ^{9}C,^{15}C,^{16}C, ^{17}C and ^{19}C using HO+LST technique are presented in Table 5 and compared with available experimental data. Unfortunately, there are no available experimental proton, charge, neutron and matter rms radii for ^{9}C, therefore, the calculated radii are compared with theoretical result of ref. [26].

In Table 6, the calculated proton, charge, neutron, matter rms radii for Carbon isotopes ^{12}C, ^{13}C and ^{22}C using LST technique are shown and compared with available experimental data. In Table 7, the same quantities calculated in Table 5, but using HO technique. The HO size parameters for protons and neutrons (b_p and b_n) are chosen so as to reproduce the experimental rms radii.

Table 5: Calculated proton, charge, neutron, matter rms radii in Fermi's for Carbon isotopes ^{9}C,^{15}C,^{16}C,^{17}C, ^{19}C by using HO+LST technique compared with available experimental data.

$^{A}_{Z}X_{N}$	b_p (fm)	b_n (fm)	$\langle r^2\rangle_p^{1/2}$	**Theo. + Exp.** $\langle r^2\rangle_p^{1/2}$	$\langle r^2\rangle_{ch}^{1/2}$	$\langle r^2\rangle_n^{1/2}$	$\langle r^2\rangle_m^{1/2}$	**Theo. + Exp.** $\langle r^2\rangle_m^{1/2}$
$^{9}_{6}C_{3}$	1.639	1.599	2.682	2.684 [26]	2.773	2.165	2.522	2.522 [26]
$^{15}_{6}C_{9}$	1.59	1.6	2.340	2.37(3) [27]	2.437	2.721	2.576	2.54(4) [27]
$^{16}_{6}C_{10}$	1.604	1.61	2.361	2.40(4) [27]	2.453	3.048	2.81	2.756(58) [11]
$^{17}_{6}C_{11}$	1.645	1.799	2.421	2.42(4) [27]	2.507	2.928	2.759	2.76(3) [27]
$^{19}_{6}C_{13}$	1.631	1.736	2.401	2.40(3) [27]	2.483	3.455	3.160	3.16(7) [27]

Table 6: Calculated proton, charge, neutron, matter rms radii in Fermi's for stable Carbon isotopes ^{12}C, ^{13}C, by using LST technique compared with available experimental data.

$^{A}_{Z}X_{N}$	b_p (fm)	b_n (fm)	$\langle r^2\rangle_p^{1/2}$	**Exp.** $\langle r^2\rangle_p^{1/2}$	$\langle r^2\rangle_{ch}^{1/2}$	**Exp.** $\langle r^2\rangle_{ch}^{1/2}$	$\langle r^2\rangle_n^{1/2}$	$\langle r^2\rangle_m^{1/2}$	**Exp.** $\langle r^2\rangle_m^{1/2}$
$^{12}_{6}C_{6}$	1.594	1.594	2.358	2.33(1) [27]	2.465	2.464(12) [28]	2.358	2.358	2.35(2) [11]
$^{13}_{6}C_{7}$	1.563	1.652	2.336	2.32(1) [27]	2.440	2.440(25) [28]	2.489	2.42	2.42(24) [11]
$^{22}_{6}C_{16}$	2.1	2.8	3.093	___	3.176	___	6.698	5.94	5.4±0.9 [29]

Table 7: Calculated proton, charge, neutron, matter rms radii in Fermi's for Carbon isotopes ^{9}C, ^{12}C, ^{13}C, ^{15}C, ^{16}C, ^{17}C and ^{19}C by using HO technique compared with available experimental data.

$^{A}_{Z}X_{N}$	b_p (fm)	b_n (fm)	$\langle r^2\rangle_p^{1/2}$	**Theo. + Exp.** $\langle r^2\rangle_p^{1/2}$	$\langle r^2\rangle_{ch}^{1/2}$	$\langle r^2\rangle_n^{1/2}$	$\langle r^2\rangle_m^{1/2}$	**Exp.** $\langle r^2\rangle_m^{1/2}$
$^{9}_{6}C_{3}$	1.819	1.599	2.677	2.684 [26]	2.782	2.165	2.518	2.522 [26]
$^{15}_{6}C_{9}$	1.59	1.736	2.340	2.37(3) [27]	2.436	2.720	2.575	2.54(4) [27]
$^{16}_{6}C_{10}$	1.604	1.927	2.361	2.40(4) [27]	2.452	3.047	2.809	2.756(58) [11]
$^{17}_{6}C_{11}$	1.645	1.809	2.421	2.42(4) [27]	2.507	2.927	2.759	2.76(3) [27]
$^{19}_{6}C_{13}$	1.631	2.086	2.401	2.40(3) [27]	2.479	3.454	3.16	3.16(7) [27]

In Table 8, the calculated proton, charge, neutron, matter rms radii for stable Carbon isotopes ^{12}C and ^{13}C using HO technique are presented and compared with available experimental data.

Table 8: Calculated proton, charge, neutron, matter rms radii in Fermi's for stable carbon isotopes ^{12}C, ^{13}C, by using HO technique compared with available experimental data.

$^{A}_{Z}X_{N}$	b_p (fm)	b_n (fm)	$\langle r^2\rangle_p^{1/2}$	Exp. $\langle r^2\rangle_p^{1/2}$	$\langle r^2\rangle_{ch}^{1/2}$	Exp. $\langle r^2\rangle_{ch}^{1/2}$	$\langle r^2\rangle_n^{1/2}$	$\langle r^2\rangle_m^{1/2}$	Exp. $\langle r^2\rangle_m^{1/2}$
$^{12}_{6}C_{6}$	1.457	1.456	2.357	2.33(1) [27]	2.464	2.464(12) [28]	2.355	2.356	2.35(2) [11]
$^{13}_{6}C_{7}$	1.449	1.476	2.336	2.32(1) [27]	2.440	2.440(25) [28]	2.489	2.42	2.42(24) [11]

The calculated MDDs are represented in Figs. 1 (a), (b), (c), (d) and (e) for ^{9}C, ^{15}C, ^{16}C, ^{17}C and ^{19}C isotopes, respectively. In Fig. 1 (a), the solid, dotted and dashed curves represent the calculated MDDs using HO+LST, LST and HO, respectively. It is clear that the results of HO+LST is in excellent agreement with experimental data and these are attributed to the generated tails coming from the used THO wavefunctions which are highly improved by the parameters in Table 3 and 4. The result of LST using NCSM calculations is not adequate to reproduce the tail and underestimates such region. In Fig.1(b), (c), (d), and (c), the solid and dashed curves represent the calculated MDDs in HO+LST and HO, respectively. In general, it is obvious that there are a very good agreements when compared with experimental data in HO+LST technique. The results of HO is completely failed in all isotopes to regenerate the long tail behaviour. In Fig.1(f), the calculated proton and neutron density distributions are depicted for ^{22}C using LST technique with assumed filling numbers (ξ). It is evident there is a very good agreement for both proton and neutron densities in comparison with experimental data.

The neutron and proton density distributions for ^{9}C, ^{15}C, ^{16}C, ^{17}C and ^{19}C are described in Fig. 2(a), (b), (c), (d) and (e), respectively. It is obvious that the long tail characteristic is well produced in the proton density distribution for ^{9}C, besides in the neutron density distribution for ^{15}C, ^{16}C, ^{17}C and ^{19}C.

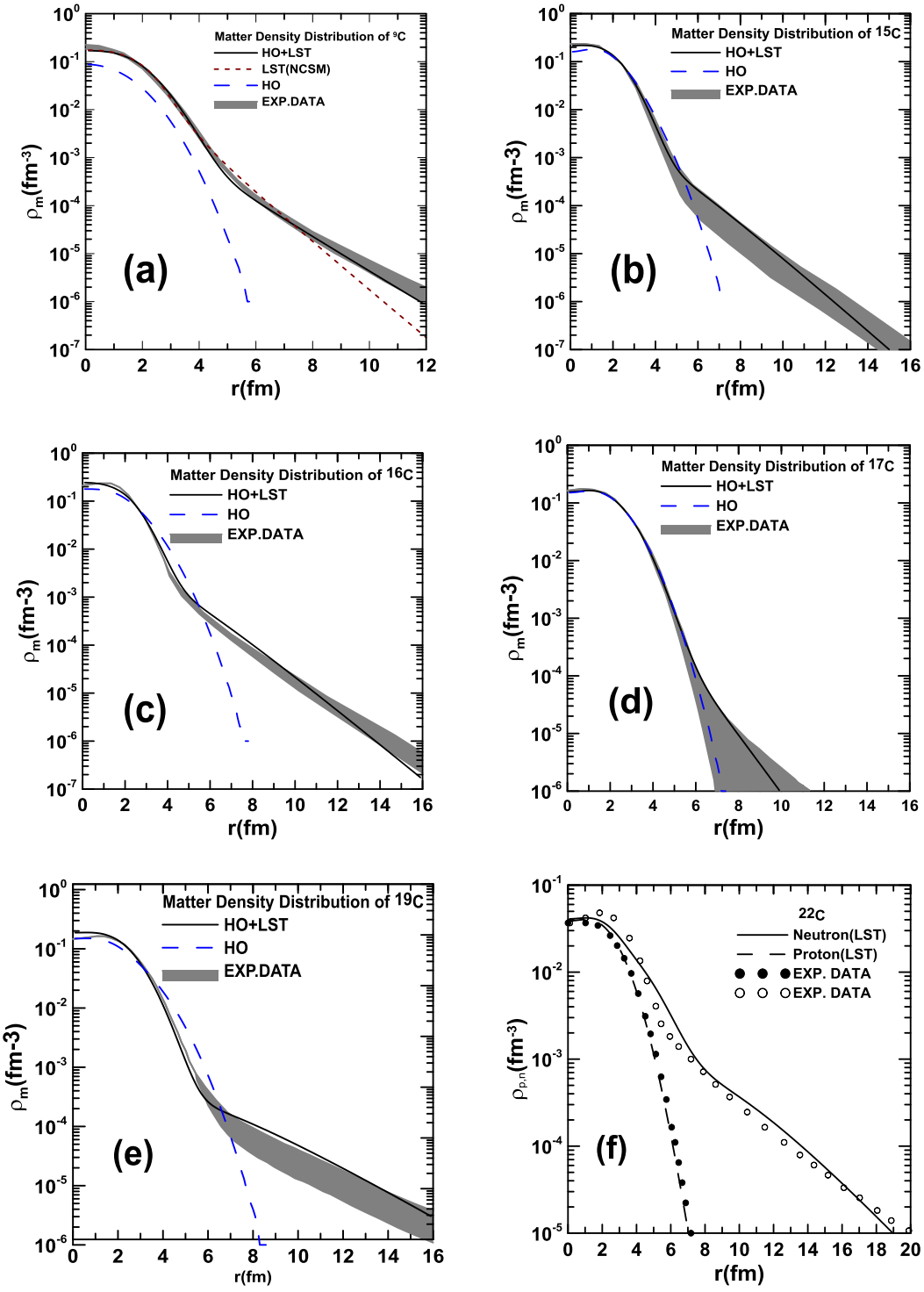

Fig. 1: The calculated MDDs for exotic Carbon isotopes ^{9}C(a) [30], ^{15}C(b), ^{16}C(c), ^{17}C (d) and ^{19}C(e) [11], represented by solid and dashed curves, respectively. The shaded areas are experimental data. ^{22}C(f), represent the neutron and proton density distribution and compared with experimental data represent by filled and empty [29] circles.

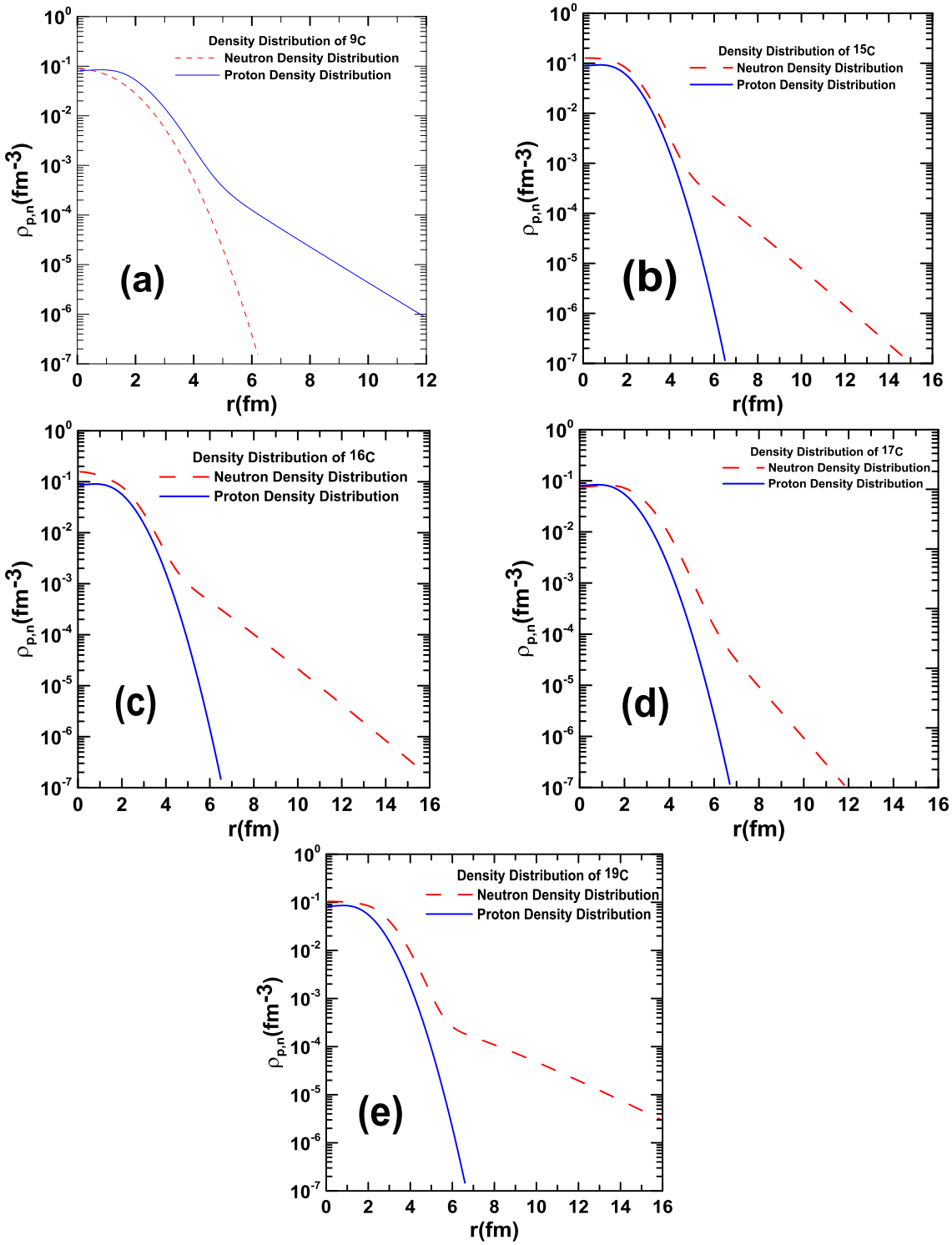

Fig. 2: The neutron and proton density distributions for carbon isotopes $^{9}C(a),^{15}C(b),^{16}C(c),^{17}C(d),^{19}C(e)$.

In Fig. 3 (a) and (b) the calculated and experimental charge density distributions of ^{12}C and ^{13}C, respectively. The solid, dotted and dashed curves represent the calculated CDD in LST, assumed ξ and HO calculations, respectively. It is evident that the calculations in LST with assumed filling numbers (ξ) are going very well with experimental data, while the results of LST in NCSM for both isotopes overestimates the results at central region.

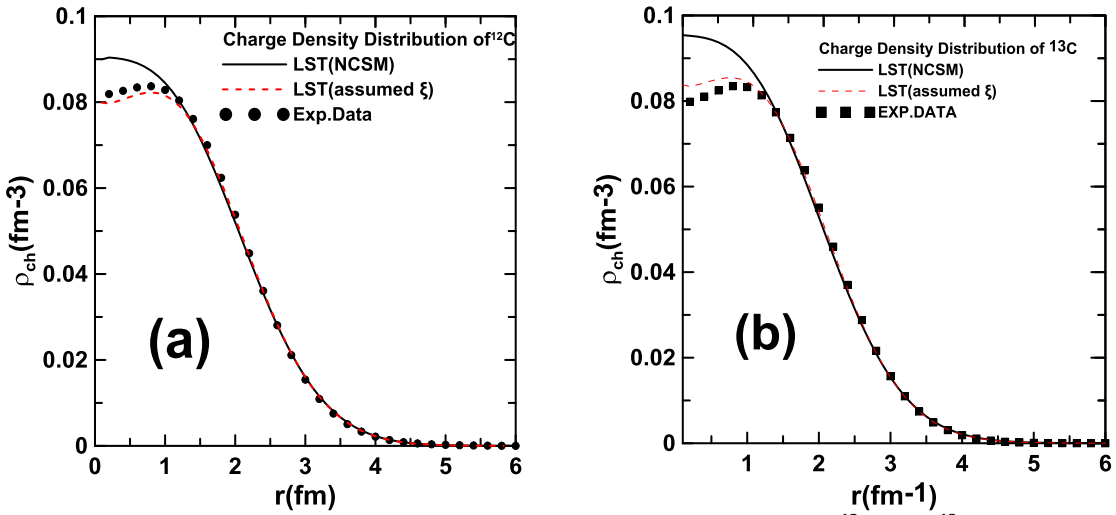

Fig. 3: (a) Charge density distributions of stable Boron isotopes ^{12}C and ^{13}C [28].

In Fig. 4 (a) and (b), the calculated and experimental charge form factors of ^{12}C and ^{13}C are depicted. The solid, red dotted and dashed curves for both nuclei represent the calculated charge form factors in LST (NCSM), LST (assumed ξ) and HO, respectively. It is obvious that the calculations in LST (NCSM) for both isotopes are shifted slightly the first diffraction minima forwards and downwards.

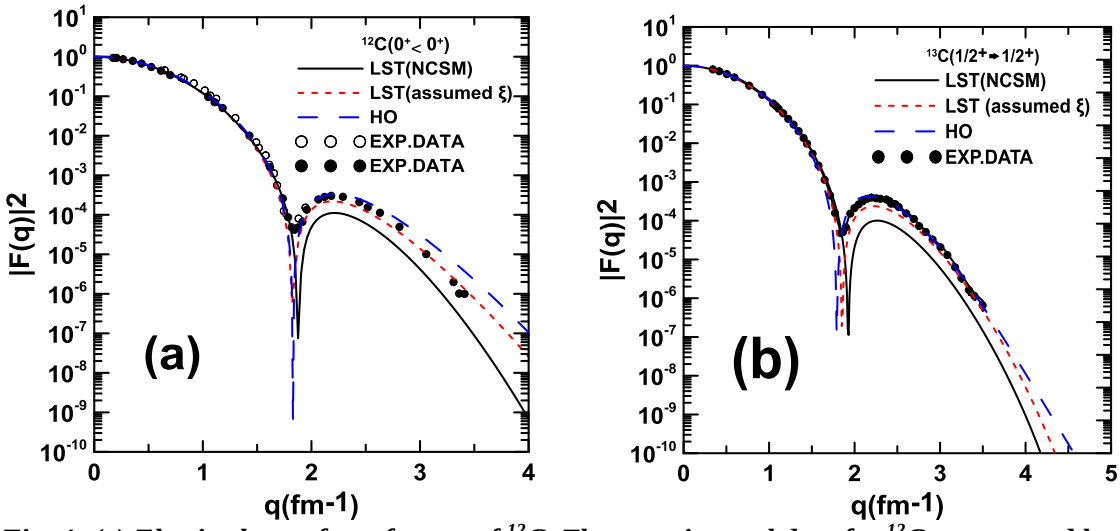

Fig. 4: (a) Elastic charge form factors of ^{12}C. The experimental data for ^{12}C represented by empty and filled circles [31]. (b) Elastic charge form factors of ^{13}C.The experimental data for ^{13}C represented filled circles [31].

Conclusions

The nuclear proton, charge, neutron, and matter density distributions and charge form factor are studied for stable (^{12}C and ^{13}C) and exotic (^{9}C, ^{15}C, ^{16}C, ^{17}C, ^{19}C and ^{22}C) isotopes. The calculations are based mainly on the (THO) wavefunctions in (LST). The HO and THO parameters needed to accomplish the calculations are chosen so as to reproduce the available experimental root-mean square (rms) proton, charge, neutron and matter radii. The results of the first approach (LST technique) used only for ^{9}C, ^{12}C, ^{13}C and ^{22}C are in very good agreement in comparison with experimental data. In the second approach (HO+LST) used only for ^{9}C,

^{15}C, ^{16}C, ^{17}C and ^{19}C, the results are greatly reformed in comparison with experimental data. The results of HO technique wavefunctions are completely failed to reproduce the long tail. Besides, the LST are applied to calculate charge density distributions of the ^{12}C and ^{13}C isotopes in order to validate the reality of using these wavefunctions. The results are highly improved using assumed filling numbers instead of those coming from using model interaction. Finally, the calculated charge form factors for ^{12}C and ^{13}C are clearly in very good agreement with experimental data using the THO in LST indicating the reality of using such approach in studying both stable and exotic nuclei.

References

[1] J. W. Negele and Erich Vogt., Adv. Nucl. Phys. 19 (1989) 1.
[2] A. Bohr and B.R. Mottelson, "Nuclear structure / Vol. 1, Single-particle motion", New York [etc.]: Benjamin, (1969).
[3] I. Tanihata, H. Hamagaki, O. Hashimoto, Y. Shida, N. Yoshikawa, K. Sugimoto, O. Yamakawa, T. Kobayashi, N. Takahashi, Phys. Rev. Lett., 55 (1985) 2676-2679.
[4] B.A. Brown, Phys. Rev. Lett., 85, 25 (2000) 5296-5299.
[5] W. E. Otten, Nuclear Radii and Moments of Unstable Isotope, Treatise of Heavy-Ion Physics. Vol. 8, Plenum Press, New York (1987).
[6] P. G. Hansen, A. S. Jensen, B. Jonson, Annu. Rev. Nucl. Sci., 45 (1995) 591-634.
[7] P. G. Hansen and B. Jonson, Europhys. Lett., 4 (1987) 409-414.
[8] K. Riisager, A. S. Jensen, P. Møller, Nucl. Phys., A 548, 3 (1992) 393-413.
[9] I. Tanihata. Neutron halo nuclei. J. Phys., G 22 (1996) 157-198.
[10] A. Ozawa, T. Suzuki, I. Tanihata. Nuclear size and related topics. Nuclear Physics A, 693 (2001) 32-62.
[11] M.V. Zhukov, B. V. Danilin, D. V. Fedorov, J. M. Bang, I. J. Thompson, J. S. Vagen, Phys. Rep., 231 (1993) 151-199.
[12] A. R. Ridha and M. K. Suhayeb. Iraqi Journal of Science, 58, 4B (2017) 2098-2106.
[13] G. R. Satchler, Direct Nuclear Reactions, Oxford University Press (1983).
[14] B. A. Brown and W. D. M Rae, MSU-NSCL Report (2007).
[15] Adel K. Hamoudi, Raad A. Radhi, Arkan R. Ridha, Iraqi Journal of Physics, 10, 19 (2012) 26-34.
[16] S. Karataglidis and K. Amos. Phys. Rev C, 71 (2005) 1-13.
[17] T. W. Donnelly, J. Dubach, Ingo Sick, Nucl. Phys., A 503, 3-4 (1989) 589-916.
[18] L. R. B. Elton; "Nuclear Sizes", Oxford University Press (1961).
[19] H. Chandra and G. Sauer, Phys. Rev., C13 (1975) 245-252.
[20] A. Trzcinska, J. Jastrzebski, P. Lubinski, F. J. Hartmann, R. Schmid, T. von Egidy. Phys. Rev. Lett., 87, 082501 (2001).
[21] T. Deforest, Jr. and J. D.Walecka, Adv. Phys. 15, 1 (1966) 1-109.
[22] B. A. Brown, B. H. Wildenthal, C. F. Williamson, F. N. Rad, S. Kowisiki, H. Crannell, J. T. O' Brien, Phys. Rev., C 32 (1985) 1127-1145.
[23] G. Audi, F.G. Kondev, Meng Wang, W.J. Huang and S. Naimi. Chinese Physics C, 41 (2017) 1-138.
[24] I. Tanihata, H. Savajols, R. Kanungo. Progress in Particle and Nuclear Physics, 68 (2013) 215-313.
[25] A. S. Jensen, K. Riisager, D. V. Fedorov, Reviews of Modern Physics, 76 (2004) 215-261.
[26] H. Rui, L. Jia-Xing, Y. Jian-Ming, J. Juan-Xia, W. Jian-Song, H. Qiang. Chain. Phys. Lett., 27, 9 (2010) 09210.1

[27] R. Kanungo, W. Horiuchi, G. Hagen, G. R. Jansen, P. Navratil, F. Ameil, J. Atkinson, Y. Ayyad, D.Cortina-Gil, I. Dillmann, A. Estrade, A. Evdokimov, F. Farinon, H. Geissel, G. Guastalla, R.Janik, M. Kimura, R. Knobel, J. Kurcewicz, Yu. A. Litvinov, M. Marta, M. Mostazo, I. Mukha, C.Nociforo, H.J. Ong, S. Pietri, A. Prochazka, C. Scheidenberger, B. Sitar, P. Strmen, Y. Suzuki, M. Takechi, J. Tanaka, I. Tanihata, S. Terashima, J. Vargas, H. Weick, J. S Win-eld, Phys. Rev. Lett., 117 (2016) 1-5.

[28] H. De Vries, C. W. De Jager, C. De Vries. Atomic Data and Nuclear Data Tables, 36, 3 (1987) 495-536.

[29] K. Tanaka, T. Yamaguchi, T. Suzuki, T. Ohtsubo, M. Fukuda, D. Nishimura, M. Takechi, K. Ogata, A. Ozawa, T. Izumikawa, T. Aiba, N. Aoi, H. Baba, Y. Hashizume, K. Inafuku, N. Iwasa, K. Kobayashi, M. Komuro, Y. Kondo, T. Kubo, M. Kurokawa, T. Matsuyama, S. Michimasa, T. Motobayashi, T. Nakabayashi, S. Nakajima, T. Nakamura, H. Sakurai, R. Shinoda, M. Shinohara, H. Suzuki, E. Takeshita, S. Takeuchi, Y. Togano, K. Yamada, T. Yasuno, M. Yoshitake, Phys. Rev. Lett., 104, 6 (2010) 062701-062704.

[30] M. Fukuda. Nucleon density distributions of unstable nuclei extracted from reaction cross sections. Soryushiron KenIKyu. C20 (N11-Electronic Library Service).

[31] I. Sick and J.S. McCarthy, Nuclear Physics, A 150 (1970) 631-654.